Imaging synaptosomal calcium concentration microdomains and vesicle fusion by using total internal reflection fluorescent microscopy

Yafell Serulle*†‡, Mutsuyuki Sugimori*‡§, and Rodolfo R. Llinás*‡§¶

*Program in Neuroscience and Physiology, †Department of Biochemistry, and §Department of Physiology and Neuroscience, New York University School of Medicine, New York, NY 10016; and ‡Marine Biological Laboratory, Woods Hole, MA 02543

Contributed by Rodolfo R. Llinás, December 4, 2006 (sent for review November 10, 2006)

Transmitter release at chemical synapses is triggered by high calcium concentration microprofiles at the presynaptic cytosol. Such microprofiles, generated by the opening of voltage-dependent calcium channels at the presynaptic plasma membrane, have been defined as calcium concentration microdomains. Using total internal reflection fluorescent microscopy in conjunction with calcium and vesicular release indicator dyes, we have directly visualized the close apposition of calcium concentration microdomains and synaptic release sites at single synaptic terminals from the CNS from rat cerebellar mossy fiber and squid optic lobe. These findings demonstrate the close apposition of calcium entry and release sites and the dynamics of such site locations over time. Kinetic analysis shows that vesicles can be released via two distinct mechanisms: full-fusion and kiss-and-run. Calcium triggers vesicular motion toward the membrane, and the speed of such movement is calcium concentration-dependent. Moreover, the immediately available vesicular pool represents molecularly trapped vesicles that can be located at a larger distance from the plasma membrane than the field illuminated by total internal reflection fluorescent microscopy.

cerebellum | mossy fibers | squid | synaptic vesicles

At most chemical synapses, vesicle fusion and transmitter release are triggered by a rise in intracellular free Ca^{2+} concentration ($[Ca^{2+}]_I$) resulting from the opening of plasmalemmal voltage-gated Ca^{2+} channels (VGCC) at the presynaptic active zone (1). Kinetic modeling initially suggested that the presynaptic $[Ca^{2+}]_I$ rises very rapidly in the immediate vicinity of Ca^{2+} channels when they open and falls equally fast as the channels close (2). The sites in the cytoplasm for these compartmentalized high calcium concentration profiles have been defined as "calcium concentration microdomains" (CCMs) (3). Because of the high calcium concentration required to trigger vesicle fusion, the rapid rise and fall of $[Ca^{2+}]_I$ after Ca^{2+}-channel opening, and the restricted spatial extension of a CCM, it has been suggested that transmitter release must take place at a site very close to the CCM. Direct evidence of these CCMs originally was obtained by using a low-affinity calcium indicator (n-aquorin-J) and a fast imaging technique in the squid giant synapse (3). Those findings indicated that those dissipative domain structures are strategically located at or near the active zone, have a dynamic time course of ≈0.8 msec, and serve as the direct trigger mechanism for transmitter release (3, 4). However, imaging techniques limitations have hampered further characterization of these CCMs and their direct correlation with transmitter release sites.

Total internal reflection fluorescent microscopy (TIRFM) allows the imaging of cellular events that take place at, or near, the plasma membrane (5) and has been used to visualize calcium entry sites (5–8) and exocytosis (9–11) in various cell types. To characterize further the CCMs and to relate them to the active zone (release site), we isolated synaptic terminals from the squid optic lobe and from rat cerebellar mossy fibers. Although there is good evidence to assume that CCMs and release sites colocalize strictly, a direct demonstration is lacking. We have approached this problem by sequentially imaging vesicle fusion and calcium entry in the same synaptosome. This was accomplished by combining calcium indicators and fluorescent dyes with TIRFM and a fast, highly light-sensitive CCD camera. Here, we provide direct evidence for the activation of CCMs during synaptosomal depolarization, their localization stability, and their banishment by specific Ca^{2+}-channel blockers. Kinetic analysis of vesicle exocytosis demonstrates two distinct modes of exocytosis: full fusion and kiss-and-run. We have found that docking and fusion are independent processes, both dependent on calcium. Moreover, calcium regulates the speed at which vesicles approach the plasma membrane before the vesicles undergo fusion. The rate at which the vesicles appear in the fluorescent field within a particular calcium concentration after depolarization was constant, suggesting that the immediately available pool represents "molecularly trapped" vesicles that can be located at a distance larger than the fluorescent field excited by the evanescent wave.

Results

Synaptosomal preparations have been shown to contain active functional presynaptic terminals (12–14) and, ultrastructurally, intact active zones (15).

Depolarization-Induced Change of Fluorescence in Synaptosomes Loaded with Calcium Dye. Plated synaptosome from squid optic lobe (Fig. 1*A*) and rat cerebellum (Fig. 1*B*) may be compared before (Fig. 1 *Ai* and *Bi*) and after (Fig. 1 *Aii* and *Bii*) loading with the cell-permeable fluorescent calcium indicator calcium green-1 (CG-1). KCl-induced depolarization generated discrete fluorescence spots (Fig. 1 *Aiii* and *Biii*), representing sites of Ca^{2+} elevation near the plasmalemma, that is, CCMs. No differences were observed in the dynamics or spatial distribution between CCMs from the squid optic lobe synaptosomes (Fig. 1*Aiii*) and those from the rat cerebellum synaptosomes (Fig. 1*Biii*).

CCMs Depend on the Opening of CaV2.1 VGCCs. Several controls were performed to confirm that the depolarization-induced fluorescence increase was due to calcium entry through VGCCs. Thus, when buffer solution was replaced for KCl, no increase in the fluorescence signal was recorded (Fig. 1*C*) ($n = 5$), confirming that depolarization was required for the fluorescence increase. Moreover, KCl application in the absence of Ca^{2+} in the bath generated no CCMs fluorescence (Fig. 1*C*). In addition, that calcium channels were responsible for this CCM activation was tested by the addition of the broad calcium channel blocker

Author contributions: M.S. and R.R.L. designed research; Y.S., M.S., and R.R.L. performed research; Y.S., M.S., and R.R.L. analyzed data; and Y.S. and R.R.L. wrote the paper.

The authors declare no conflict of interest.

Abbreviations: CCM, calcium concentration microdomains; CG-1, calcium green-1; TIRFM, total internal reflection fluorescent microscopy; VGCC, voltage-gated calcium channels.

¶To whom correspondence should be addressed. E-mail: llinar01@med.nyu.edu.

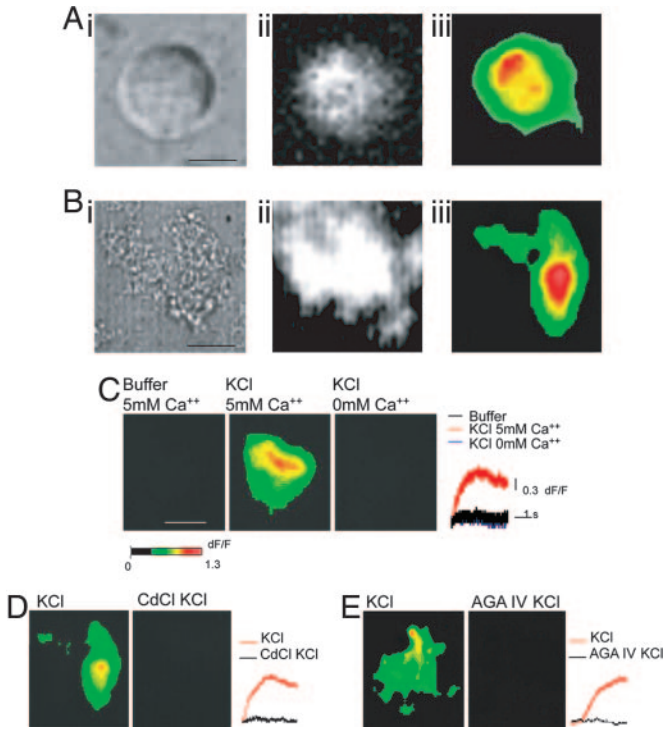

Fig. 1. Activation of CCMs in squid optic lobe and rat cerebellum synaptosomes. (*Ai*) Plated synaptosome from the squid optic lobe. (Scale bar: 2 μm.) (*Aii*) Fluorescent image of the same synaptosome shown in *Ai*, now loaded with CG-1. This image was taken at rest by using the highest laser intensity for illustration purposes. (*Aiii*) Induction of CCMs by local KCl application. Shown is an individual frame displaying the change of fluorescence in the squid optic lobe synaptosome after KCl depolarization. (*Bi*) Plated synaptosome from the rat cerebellum. (Scale bar: 4 μm.) (*C*) Calcium signal from rat cerebellum synaptosomes is reduced under conditions that abolish calcium influx. (*C Left*) There is no change of fluorescence without depolarization. (Scale bar: 4 μm.) (*C Center*) Same synaptosome as in *C Left*, but after depolarization by KCl. Depolarization induced a change of fluorescence. (*C Right*) KCl was washed out from the bath and solution was changed to 0 mM Ca^{2+}. Application of KCl did not produce any change of fluorescence when solution contained 0 mM Ca^{2+}. Time course and amplitude of optical responses of a single pixel (pixel of highest intensity) for the three stimulation conditions are shown in the traces to the right. (*D Left*) Change of fluorescence after depolarization. (*D Right*) Incubation with $CdCl_2$ (10 μM) for 10 min prevented the change of fluorescence after KCl depolarization. Time-course and amplitude of optical responses of a single pixel (pixel of highest intensity) are shown to the right for the two stimulation conditions. (*E Left*) Change of fluorescence after depolarization. (*E Right*) KCl depolarization did not induce a change of fluorescence after incubation with AGA IV (10 μM) for 10 min. Time course and amplitude of optical responses of a single pixel (pixel of highest intensity) are shown to the right for the two stimulation conditions.

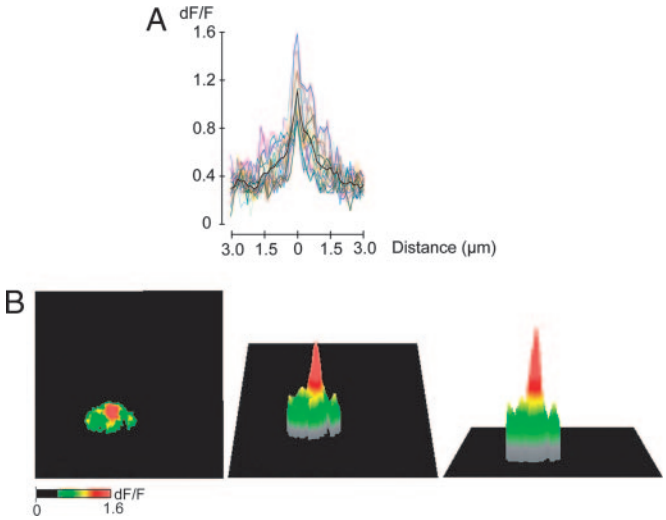

Fig. 2. Spatial profile of CCMs from squid optic lobe synaptosomes. (*A*) Profiles of 19 microdomains from 12 synaptosomes. (Black line shows the average of all traces.) The center of the Ca^{2+} influx was determined by averaging 20 frames from different time points during a single trial and then locating the pixel in which the signal was the brightest. The spatial profile of a domain was obtained by averaging the horizontal and vertical lines located through the center. (*B*) Three-dimensional projection of a CCM.

$CdCl_2$, which prevented depolarization-induced calcium entry (Fig. 1*D*) ($n = 4$), confirming that calcium entry depended on VGCCs. Furthermore, the specific CaV2.1 (P type) calcium channel blocker AGA IV abolished the calcium signals (Fig. 1*E*) ($n = 3$). This was expected because the CaV2.1 channels have been identified as implementing transmitter release in these types of terminals (16, 17).

Spatial Profile and Location Stability of CCMs. The size of the CCMs were determined by averaging the relative change of fluorescence over 24 frames during a single depolarization trial. The pixel of highest fluorescence intensity then was chosen as the center of the domain. The radius of the domain was determined by averaging the profile of horizontal and vertical lines taken across the pixel of highest intensity and plotting size as a function of the relative change of fluorescence. The average size of 19 microdomains from 12 different synaptosomes are shown in Fig. 2*A*. A representative CCM and its three-dimensional distribution is shown in Fig. 2*B*. The fluorescence intensity of a CCM and its spatial extent had a Gaussian distribution. The highest peak of intensity in a CCM was consistently concealed within an area of a single pixel ($n = 19$), which corresponds to an area of $\approx$0.15 μm^2. The fluorescence intensity decreased with distance to 73 $\pm$ 2% of the peak fluorescence 0.15 μm from the highest intensity pixel and to 48 $\pm$ 3% of the maximum 0.45 μm from the center the fluorescence in the domain. Based on fluorescence decay with respect to distance from the center, a FWHM of 990 $\pm$ 56 nm was calculated. The presence of a single peak of highest intensity in the CCM and the decrease of fluorescence in the pixels immediately adjacent to that pixel suggests that the site of calcium entry is located within the area imaged by a single pixel. The distribution of fluorescence in pixels distant from the center suggests that calcium diffused away from sites of its entry as expected by simple diffusion.

Structural work in whole terminals (18) and individual active zones (19) has suggested that interactions between calcium channels and active zone molecular elements allow the channels to be kept within very close proximity of the synaptic vesicles. In fact, several studies have shown specific molecular interactions between punctuated intracellular calcium channel profiles and cytoplasmic proteins (20, 21) and between the extracellular domains of the channels and proteins in the synaptic cleft (22). To determine the physical stability of CCMs located at a specific site in the synaptosome plasmalemma, their location was determined after prolonged stimulation. Synaptosomes were depolarized every 30 min for a period of 2–3 h. CCMs localization demonstrated remarkable stability after repeated depolarization events (6–8 events repeated every 30 min for a period of 2–3 h) ($n = 3$) (Fig. 3). We calculated the center of mass of each CCM at each depolarization event (see *Methods*) and compared the displacement of each CCM every 30 min. We found that every 30 min the center of the domain moved only 0.93 $\pm$ 0.18 μm. These results indicate that CCMs are stable structures and demonstrate minimal variability in their location over the 2- to 3-h period.

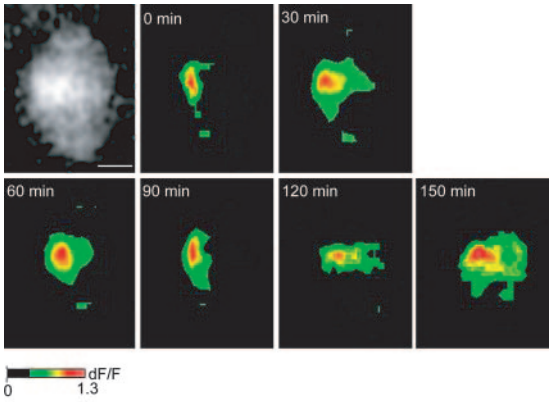

Fig. 3. Temporal stability of calcium entry sites in squid optic lobe synaptosomes. Synaptosomes were depolarized every 30 min. *Left* shows the squid optic lobe synaptosome at rest, loaded with CG-1. Subsequent panels show the same synaptosome after depolarization at different time points (top of each image). (Scale bar: 2 μm.)

Colocalization of CCMs with Release Sites. Because a high calcium concentration profile is required to trigger transmitter release, it has been proposed that vesicle fusion takes place close to the sites where calcium enters the synaptic preterminal (2). These sites are expected to be located close to the center of the CCMs (2). To determine whether this is the case, and whether CCMs colocalized with the sites of transmitter release, FM and calcium dyes imaging were combined (Fig. 4). Thus, synaptosomes were loaded initially with calcium dyes (Fig. 4*A i* and *ii*). After CCMs visualization, the calcium dye was photobleached with a high intensity laser light. Under these conditions, depolarization no longer induced an increase in fluorescence (Fig. 4*B*). This initial step was followed by synaptosomal loading with the lipophilic dye FM1-43. Depolarization now induced a discrete spot of fluorescence increase, which appeared at approximate the same site as calcium entry (Fig. 4 *C* and *D*). (Fig. 4 *Aii* and *Cii* are the same image as in Fig. 4*D*, but after thresholding the value of the pixels so that only the pixels of higher intensity can be seen. This demonstrates an excellent colocalization between sites of calcium entry and sites of vesicle fusion.

Imaging Synaptic Vesicles and Kinetics of Exocytosis. Using the FM1-43 dye, the exocytic events in our preparation were studied in more detail. Applied at the concentration used in the present study, FM1-43 has been shown to stain 1–2% of the synaptic vesicles present in the synaptic terminal (23). Moreover, when imaged by TIRFM, FM1-43 dye has been shown to give the resolution of single vesicles (24). Staining of synaptosomes with FM1-43 produced single fluorescent spots in the plasma membrane (Fig. 5 *A* and *B*). In some cases, depolarization with KCl induced the disappearance of these spots (Fig. 5*A*), as if vesicles that were docked at the membrane fused and, therefore, lost the dye. In other cases, depolarization by KCl induced the appearance of new vesicles (Fig. 5*B*), which, after achieving a peak fluorescence, eventually disappeared (Fig. 5*B*), suggesting that depolarization induced the arrival of new vesicles to the evanescent field and that these vesicles underwent fusion. Finally, in some instances, vesicles appeared in the fluorescent field but did not lose any dye (data not shown), as if they would not fuse, or vesicles that were initially docked did not fuse after depolarization. To analyze in detail the exocytosis events, we looked at the kinetics of single fluorescent spots (see *Methods*). Fig. 5 *C* and *D* show vesicles that were docked initially and fused after depolarization, and Fig. 5 *E* and *F* show vesicles that appeared in the evanescent field after depolarization and later fused. In the examples shown on Fig. 5 *C* and *D*, depolarization was followed

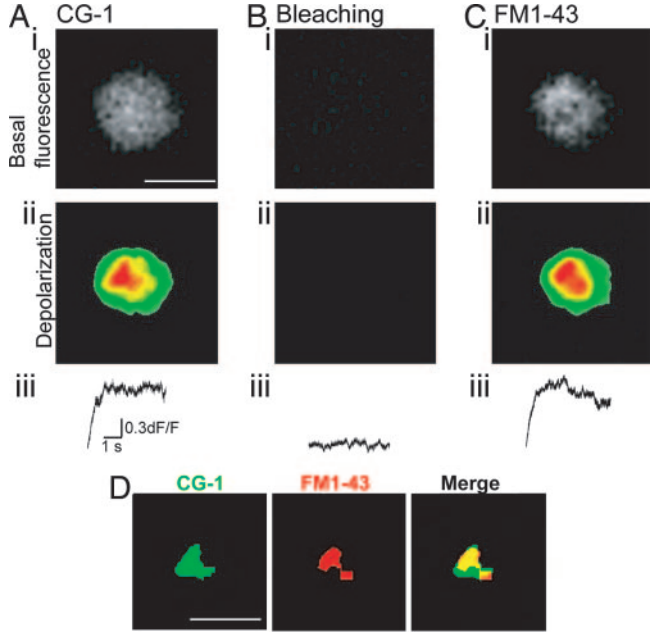

Fig. 4. Colocalization of CCMs with release sites in squid optic lobe synaptosome. (*Ai*) A squid optic lobe synaptosome at rest and loaded with the calcium dye CG-1. (Scale bar: 4 μm.) (*Aii*), Fluorescence change in the same synaptosome as in *Ai* after depolarization, showing the presence of CCM. (*Aiii*) Time course and amplitude of the optical response of a single pixel (pixel of highest intensity) from the trial shown in *Aii*. (*Bi*) Same synaptosome as in *Ai* at rest. After recording the depolarization-induced calcium optical signals shown in *A*, high laser intensity was used to induce bleaching of the calcium dye CG-1. No basal fluorescence was seen after photo bleaching. (*Bii*) After bleaching of the dye, changes in fluorescence after depolarization were no longer observed. (*Biii*) Time course and amplitude of the optical response of a single pixel (pixel of highest intensity) from the trial shown in *Bii*. (*Ci*) After photo bleaching, synaptosome was loaded with the dye FM1-43. The image shows fluorescence of the dye at rest. (*Cii*) Depolarization induced a change in fluorescence intensity. (*Ciii*) Time course and amplitude of the optical response of a single pixel (pixel of highest intensity) from the trial shown in the *Cii*. (*D*) Same experiment as in *A*–*C*. To better visualize the colocalization of the CCM with the release site, the images were thresholded so that only the pixels of highest intensity are shown. (*D Left*) Signal from CG-1, shown in green. (Scale bar: 2 μm.) (*D Center*) Signal from FM1-43, shown in red. (*D Right*) Merging of *D Left* and *Center* to show the colocalization of the CG-1 and FM1-43 signals. Colocalized pixels of both images are shown in yellow.

by a decrease in fluorescence, whereas in the examples in Fig. 5 *E* and *F*, depolarization was followed first by an increase in fluorescent and then by a decrease. We noticed that both in the vesicles that were initially docked and in the vesicles that appeared in the evanescent field right after depolarization, the decay time of fluorescence fell into two separate groups, those in which the decay was fast ($\approx$300 ms) and those in which the decay was slow ($\approx$3 s). Fig. 5 *G* and *H* show the average decay time of several events of each of these two groups. The difference in decay time suggests different mechanisms by which the FM dye is released from vesicles once the vesicles fuse. In fact, it has been shown that the slow release of FM dye from synaptic vesicles may be mediated by a narrow fusion pore (25), suggesting "kiss-and-run" exocytosis, whereas the fast release is consistent with full fusion of the vesicle (25, 26). These results show that in CNS synaptosomes both kiss-and-run and full fusion-mediated transmitter release is operant.

Next we compared the time of rise of fluorescence of vesicles that were not docked initially but appeared in the evanescent field after depolarization. There was no significant difference in the time of rise between those vesicles that later underwent fusion and those

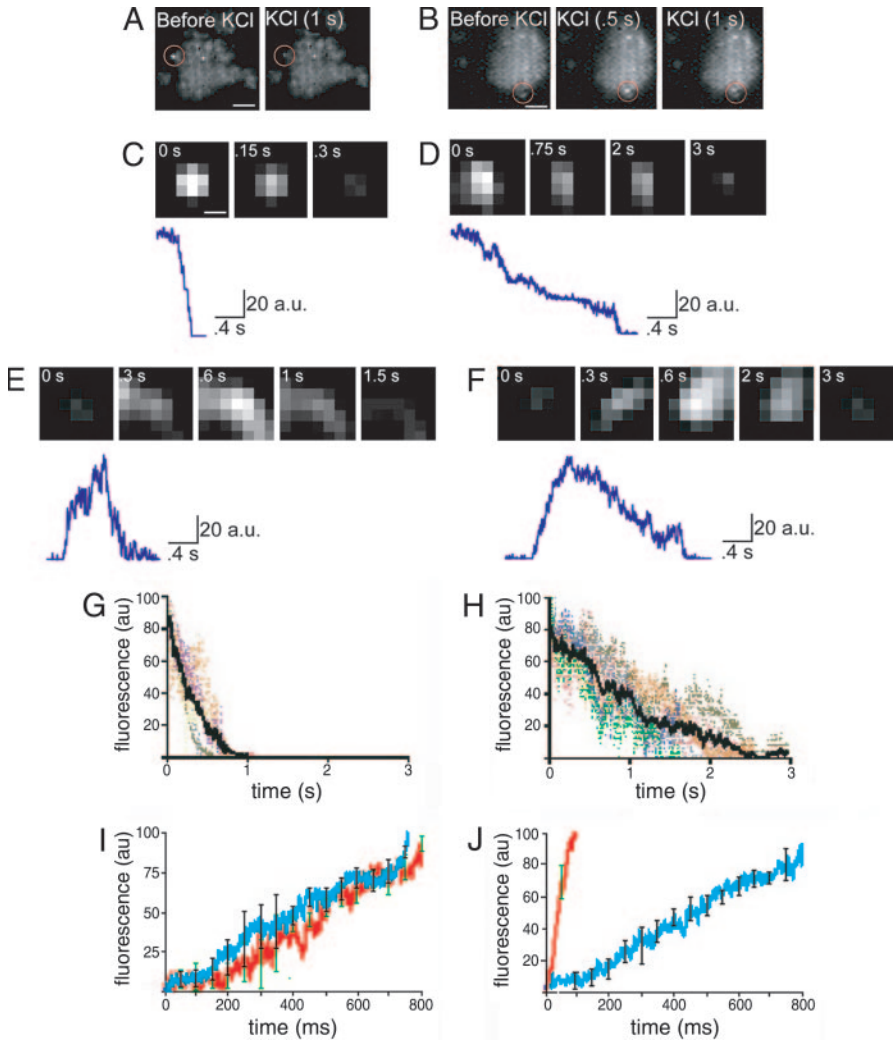

Fig. 5. Different mechanisms of vesicle fusion. (*A*) Single video frames showing a cerebellar synaptosome loaded with FM1-43 dye and imaged by TIRFM. Circled in red is a fluorescent spot that was present initially and which disappeared after depolarization by KCl. (Scale bar: 1.5 μm.) (*B*) Single video frames showing a synaptosome loaded with FM1-43 dye as shown in *A*. Circled in red is an area where, after depolarization with KCl, a fluorescent spot appeared (i.e., a newly docked vesicle) and later disappeared. (Scale bar: 1.5 μm.) (*C*) To analyze the kinetics of single fluorescent spots, a square around the fluorescent spot was excised and the fluorescence was fit to a 2D Gaussian function. Background then was subtracted. The fluorescent spot shown in *C* is the same as in the one inside the circle in *A*, after Gaussian fitting and background subtraction. The times shown at the top refer to the times after depolarization. (Scale bar: 0.30 μm.) Same scale was used for *D–F*. At the bottom of *C–F*, the trace show the kinetics of the optical signal measured at the center of the fluorescent spot. (*D*) A fluorescent spot similar to the one in *C*, but with different kinetics. Note the slower rate of fluorescence decay. (*E*) A fluorescent spot analyzed as in *C* and *D*, similar to the one seen in *B*. The times refer to the time after depolarization. Note that at 0.8 s after depolarization, the spot achieves peak fluorescence and then starts to decay. (*F*) A spot similar to the one in *E* but with different kinetics. Note the similar kinetics of the rising phase and the distinct kinetics of the decay. (*G*) Average time of decay of the ''full fusion'' events. In color are traces of six different experiments, and in black is an average of the six experiments. (*H*) Average time of decay of the kiss-and-run events. In color are traces of experiments from six different preparations, and in black is an average of these six experiments. (*I*) Comparison of the rise time of the full fusion events with the kiss-and-run events. Shown is the average of each group with error bars. Error bars are standard deviation of the mean. Blue with black error bars, kiss-and-run events; red with green error bars, full fusion events. No significant difference was seen in their time of rise (n = 6 different synaptosomes for each experimental group). (*J*) Comparison of the time of rise when extracellular calcium concentration was changed from 2 mM to 10 mM. Blue with black error bars, 2 mM Ca^{2+}; red with green error bars, 10 mM Ca^{2+}. Note the faster rise of the fluorescence with higher calcium concentration (n = 4 synaptosomes with 2 mM Ca^{2+} and 10 synaptosomes with 10 mM Ca^{2+}).

that went kiss-and-run (τ = 260 $\pm$ 52 ms for kiss-and-run, and τ = 349 $\pm$ 92 ms for full fusion; n = 6 for each group) (Fig. 5*I*), suggesting that the mechanism by which the vesicles arrive to the active zone is independent from the fusion event (Fig. 5*I*). We hypothesized that the docking event was mediated by calcium entry and that, in fact, increasing the amount of calcium that goes in the presynaptic terminal during depolarization would increase the rate at which the vesicles arrive to the active zone. To directly test this hypothesis, the calcium concentration in the bath was increased from 2 to 10 mM. Fig. 5*J* shows the comparison of the rise of fluorescence between 2 mM Ca^{2+} and 10 mM Ca^{2+}. At 2 mM Ca^{2+} the fluorescence rose with a τ = 290 $\pm$ 7 ms (n = 10), whereas at 10 mM Ca^{2+} with a τ = 37 $\pm$ 4 ms (n = 4), calcium regulates the docking step.

Discussion

Neurotransmitter release from the presynaptic terminal is a highly regulated event. The finding that the latency for the postsynaptic response in the squid synapse after calcium entry is $\approx$200 μsec suggested that vesicle fusion must occur very close to the site of calcium entry (27). Initial theoretical studies proposed that calcium entry through VGCCs produced high calcium concentration pro-

files that would occur at the vicinity of the inner pore of the open channel (2). The sites at the cytoplasm where this microconcentrational profiles occurred were named CCMs, and the first experimental evidence for such CCMs was obtained later in the squid giant synapse (3). Using fast imaging TIRFM with calcium indicator dyes in combination FM dyes in the same synaptosome, we have demonstrated that CCMs colocalize with the sites of synaptic vesicle fusion, i.e., transmitter release. We also have found that two different modes of exocytosis coexist in the presynaptic terminals of two different CNS, the squid optic lobe and the mammalian cerebellum, and that the rate at which the vesicles arrive at the active zone indeed is regulated by calcium and quite similar for these two phylogenetically distant cases.

Imaging of CCMs. Confirmation that the CCM images corresponded to the sites of voltage-gated calcium entry was provided by the failure of potassium depolarization to trigger calcium signals in the absence of extracellular calcium (Fig. 2*A*) and by the banishment of CCMs after the application of broad as well as specific calcium channel blockers (Fig. 2 *B* and *C*). The pharmacology of CCMs (Fig. 2*C*) is in agreement with previous findings of Ca^{2+} entry through CaV2.1 channels in these presynaptic terminals (16, 17, 28).

Size and Localization Stability of CCMs. The location of a single pixel of highest intensity within the microdomain indicates that calcium entry occurs within an area of $\approx 0.15\ \mu m^2$ or less. This can be interpreted as the physical spread of clustered VGCCs. This is a very likely conjecture because the size of an active zone fluctuates between 0.22–1.2 μm^2, and ultrastructural studies have indicated that calcium channels occupy 5–10% of the active zone area (29, 30). The distribution of the calcium cloud was calculated by determining the rate of decay of fluorescence in the pixels away from the center, which resulted in a FWHM of 990 ± 56 nm. Based on this FWHM, the spread of the fluorescence signal over a radius of 495 ± 28 nm may reflect the spread of calcium ions from the site of entry at the active zone.

Biochemical studies have suggested that VGCCs are targeted to presynaptic sites by specific protein–protein interactions that involve both the intracellular and extracellular channel domains (20, 22). Disruption of the interaction between the synaptic protein interaction (synprint) sites in the II-III loops of α_1 subunits of CaV2.1- and CaV2.2 channels with SNARE proteins has been shown to reduce release effectiveness, providing evidence for the importance of location proximity in these release events (20). It also has been proposed that there are specific presynaptic molecular "slots" for CaV2.1 VGCCs and that the number of these slots are limited (31), giving further evidence of the high regulation of the location of these channels at the presynaptic terminal. Consistent with these results, we have found that CCMs remained at the same location throughout experiments in which the same synaptosome was depolarized for periods exceeding 2 h.

It also has been suggested that synaptic targeting of certain VGCCs requires appropriate contact between the presynaptic terminal and postsynaptic neuron (32). Although in some cases we saw structures that suggested the presence of linked pre- and postsynaptic terminals, we limited the majority of our studies to those terminals that did not have any corresponding postsynaptic structure. Our results suggest that interactions between presynaptic and postsynaptic structures are not required for keeping VGCCs at their strategic sites in the active zone. Although these results do not address the types of mobility demonstrated during synaptic development, they do support studies that indicate synaptic stability in the mature brain.

Two Different Modes of Exocytosis. Increasing evidence has shown that two different modes of exocytosis mediate secretion from vesicles, one in which there is full vesicle fusion and another one that has been named kiss-and-run, where a transient fusion pore connects the lumen of the vesicle to the extracellular space and vesicular contents are released without the vesicle fully collapsing into the plasma membrane (33, 34). Although in neuroendocrine cells it has been well established that both mechanisms mediate exocytosis (35, 36), technical limitations have prevented the study of synaptic vesicles, which tend to be of smaller size. Recently, using various imaging techniques, it has been shown that in hippocampal neuronal terminals, both mode of exocytosis coexist (25, 37, 38). Our results are in agreement with these studies. Here we have shown that both in the synaptic preterminal of the squid optic lobe and in the cerebellar mossy fibers, exocytosis takes place through both full vesicle fusion and kiss-and-run.

The combination of FM1-43 dye and TIRFM has proved to be a powerful tool to image directly vesicle fusion at the retinal bipolar neuron presynaptic terminal (24, 26). However, TIRFM has been difficult to implement at presynaptic terminals of the mammalian CNS because of their small size. We have circumvented this problem by isolating synaptic preterminals in a synaptosomal preparation from mossy fiber, one of the largest terminal types in mammalian CNS. CNS synaptososmes indeed have been shown to preserve the presynaptic machinery necessary for vesicle exocytosis and transmitter release (14).

Based on the rate of efflux of the FM1-43 dye from the synaptic vesicle, Richards *et al.* (25) analyzed the kinetics of single vesicles in hippocampal terminals. They found events that showed a fast decay (rapid destaining of the vesicle after depolarization), corresponding to a full and rapid loss of vesicular FM1-43, and events that showed a slower decay, corresponding to a partial, slow loss of dye. These two groups formed two separate clusters. In agreement with their results, we have found that the time at which vesicles destained have two time constants: slow ($\approx$300 ms) and fast ($\approx$3 s), representing the time at which the FM dye left the vesicle. Of note, the fast events described by Richards *et al.* (25) occurred with $\tau = 600$ ms, approximately twice as slow than in our study. This may reflect a difference in imaging techniques and also a difference in the sampling time. Interestingly, the large events described in that study showed a broad distribution of decay rates ($\tau = 3$–7 s), suggesting a wide variation in fusion pore size.

Vesicle "Docking" and Calcium Concentration. Our results show that after depolarization, in the presence of calcium, new vesicles appeared in the evanescent field. In these cases, vesicle destaining (fluorescence decay) was preceded by an increase in fluorescence, which, after achieving a peak intensity, rapidly decayed. The decay times of these newly arriving vesicles fell into the same groups of those that were initially docked, namely, slow and fast decay. The previously undescribed observation here is the fact that the appearance of fluorescent vesicles into the evanescence space, after depolarization, occurs within a rather sharp time delay for all cases where this event was observed ($n = 15$). Of these, the time courses were determined for extracellular Ca^{2+} concentrations of 2 mM ($n = 10$) and 10 mM ($n = 4$). The time course between depolarization and fluorescence increase was 290 ± 7 ms for the 2 mM cases and 37 ± 4 ms for the 10 mM concentration. The rise in fluorescence likely reflects the entrance of the vesicle into the evanescent field. The constancy of this rate of fluorescence increase within a particular calcium concentration suggests that (*i*) the immediately available vesicular pool represents molecularly trapped vesicles and suggests the possibility that these trapped vesicles may exist at a distant larger than the evanescence corridor and (*ii*) the results are also consistent with the fact that calcium triggers vesicular motion toward the membrane of those vesicles that are trapped (linked to the molecular machinery that triggers vesicular apposition against the plasma membrane and the release process itself). That the speed of such motion is increased 10-fold with a 5-fold increase of calcium concentration indicates a cooperative molecular event for this phenomenon. Because we also

found that the time to rise was comparable for vesicles undergoing full fusion (fast decay) and those implementing kiss-and-run release (slow decay), we conclude that vesicular docking is neutral concerning vesicular fusion dynamics.

Materials and Methods

Synaptosomal Preparation. Cerebellar synaptosomes were prepared from rat brain as described in ref. 39, with some modifications. The cerebellum was removed quickly and homogenized in 20 ml of ice-cold 0.32 M sucrose in a glass homogenizer, and the suspension was centrifuged at $3,000 \times g$ for 3 min at 4°C. The supernatant was centrifuged at $14,600 \times g$ for 11 min at 4°C. The pellet was resuspended in 3 ml of tyrode buffer. Squid optic lobe synaptosomes were prepared from six optic lobes as described in ref. 40. Briefly, optic lobes were homogenized in 1.5 ml of ice-cold 0.7 M sucrose, buffered with 20 mM Tris·HCl to a pH 7.4. The suspension was centrifuged at $3,000 \times g$ for 11 min at 4°C, and the supernatant was centrifuged at $14,000 \times g$ for 30 min at 4°C. The pellet was resuspended in 3 ml of artificial sea water. After resuspension, cerebellar and squid optic lobe synaptosomes were plated in glass bottom dishes (Willco Wells, Amsterdam, The Netherlands) and stored for 0.5–4 h at 4°C before use.

Fluorescent Calcium Indicators and FM1-43 Loading. Synaptosomes were incubated for 45 min in solution containing 5 μM CG-1 and 20% Pluronic F-127 (Molecular Probes) at 4°C. For FM1-43 loading, synaptosomes were stained for 90 s with 4 μM FM 1-43 in 50 mM K^+ solution. After dye loading, synaptosomes were washed for at least 15 min. All experiments were performed at room temperature.

Total Internal Reflection Fluorescent Microscopy and Image Analysis. Images were acquired on an Olympus (Melville, NY) IX71 microscope equipped with a ×60, 1.45 N.A., oil-immersion objective and an Argon ion laser. Optical signals were monitored with a fast CCD camera (MiCAM ULTIMA-L) with 100 × 100 pixels of spatial resolution. The total area imaged was 15 × 15 μm, and each pixel collected light from a surface of ≈0.15 × 0.15 μm. Images were sampled every 1 ms, and optical signals were imaged for ≈4 s during each trial. For each trial, the base fluorescence (F_0) was calculated by averaging 64 frames. Changes in fluorescence were evaluated as dF/F. Optical recordings of calcium signals were analyzed by using BrainVision software (SciMedia USA), except otherwise indicated. Signals were filtered with a low-pass and "cubic" filter. The optical signals were displayed by using the RGB 256 color scale in such a way that their maximum amplitude equaled the maximum red color intensity of the scale.

For calculation of the mobility of CCMs, the distance between centers of each domain was calculated for each of two consecutive trials. The center of domain was chosen by calculating the center of mass, which is the brightness-weighted average of the x and y coordinates of all pixels in the selection, with ImageJ software (National Institutes of Health). The center of mass of each pixel usually correlated to the pixel that had the highest fluorescence intensity in a single depolarization trial.

For the analysis of vesicle exocytosis with the FM1-43 dye, images were acquired as described above and then analyzed with BrainVision software (SciMedia USA) and ImageJ software (National Institutes of Health). We defined "docked vesicles" as those fluorescent spots that had maximum fluorescence intensity in basal conditions (unstimulated). Vesicles that fused were defined as those fluorescent spots that destained after depolarization. In the cases of vesicles that were not docked, they were included for analysis only when an increase in fluorescence was followed by a decrease right after peak intensity. After choosing the fluorescent spot for analysis in the raw image, a ≈1 μm × 1 μm square was excised from the image and analyzed independently. The center of the square was the center of the fluorescent spot, which was the pixel that achieved the highest intensity during a 4-s optical recording. The image was smoothed by convolution with a Gaussian kernel of $\sigma = 2$ pixels in radius to reduce image noise. Background fluorescence was defined as the average fluorescence of the plasma membrane outside the defined fluorescent spot. This fluorescence did not change after depolarization and reflects residues in the plasma membrane of the FM1-43 dye after it has already been washed out. Only pixel intensities above background were considered as signal. For the fluorescence vs. time plots shown in Fig. 5, the center pixel of the fluorescent spot was selected and its fluorescence was measured over time. Fluorescence intensities of different experiments were normalized to the maximum intensity of each individual experiment. Time constants (τ) for both rise and decay of fluorescence were determined by fitting the curves to monoexponential curves. The t test was used to compare time constants of different groups.

We thank Michinori Ichikawa, Takashi Tominaga, and Yasuhito Yamamoto for technical assistance setting up the TIRFM system. This work was supported by National Institutes of Health Grant NS13742 (to R.R.L.).

1. Schneggenburger R, Neher E (2005) *Curr Opin Neurobiol* 15:266–274.
2. Simon SM, Llinas RR (1985) *Biophys J* 48:485–498.
3. Llinas R, Sugimori M, Silver RB (1992) *Science* 256:677–679.
4. Llinas R, Sugimori M, Silver RB (1995) *Neuropharmacology* 34:1443–1451.
5. Omann GM, Axelrod D (1996) *Biophys J* 71:2885–2891.
6. Zenisek D, Davila V, Wan L, Almers W (2003) *J Neurosci* 23:2538–2548.
7. Becherer U, Moser T, Stuhmer W, Oheim M (2003) *Nat Neurosci* 6:846–853.
8. Beaumont V, Llobet A, Lagnado L (2005) *Proc Natl Acad Sci USA* 102:10700–10705.
9. Oheim M, Loerke D, Stuhmer W, Chow RH (1998) *Eur Biophys J* 27:83–98.
10. Schmoranzer J, Goulian M, Axelrod D, Simon SM (2000) *J Cell Biol* 149:23–32.
11. Steyer JA, Horstmann H, Almers W (1997) *Nature* 388:474–478.
12. Benech J, Crispino M, Chun JT, Kaplan BB, Giuditta A (1994) *Biol Bull* 187:269.
13. Benech JC, Lima PA, Sotelo JR, Brown ER (2000) *J Neurosci Res* 62:840–846.
14. Blaustein MP, Johnson EM, Jr, Needleman P (1972) *Proc Natl Acad Sci USA* 69:2237–2240.
15. Pant HC, Pollard HB, Pappas GD, Gainer H (1979) *Proc Natl Acad Sci USA* 76:6071–6075.
16. Llinas R, Sugimori M, Lin J-W, Cherksey B (1989) *Proc Natl Acad Sci USA* 86:1689–1693.
17. McFarlane MB, Gilly WF (1996) *Proc Natl Acad Sci USA* 93:5067–5071.
18. Robitaille R, Adler EM, Charlton MP (1990) *Neuron* 5:773–779.
19. Harlow ML, Ress D, Stoschek A, Marshall RM, McMahan UJ (2001) *Nature* 409:479–484.
20. Catterall WA (1999) *Ann NY Acad Sci* 868:144–159.
21. Missler M, Zhang W, Rohlmann A, Kattenstroth G, Hammer RE, Gottmann K, Sudhof TC (2003) *Nature* 423:939–948.
22. Sunderland WJ, Son YJ, Miner JH, Sanes JR, Carlson SS (2000) *J Neurosci* 20:1009–1019.
23. Rouze NC, Schwartz EA (1998) *J Neurosci* 18:8614–8624.
24. Zenisek D, Steyer JA, Almers W (2000) *Nature* 406:849–854.
25. Richards DA, Bai J, Chapman ER (2005) *J Cell Biol* 168:929–939.
26. Zenisek D, Steyer JA, Feldman ME, Almers W (2002) *Neuron* 35:1085–1097.
27. Llinas R, Sugimori M, Simon SM (1982) *Proc Natl Acad Sci USA* 79:2415–2419.
28. Mintz IM, Sabatini BL, Regehr WG (1995) *Neuron* 15:675–688.
29. Pumplin DW, Reese TS, Llinas R (1981) *Proc Natl Acad Sci USA* 78:7210–7213.
30. Pumplin DW, Reese TS (1978) *Neuroscience* 3:685–696.
31. Cao YQ, Piedras-Renteria ES, Smith GB, Chen G, Harata NC, Tsien RW (2004) *Neuron* 43:387–400.
32. Maximov A, Bezprozvanny I (2002) *J Neurosci* 22:6939–6952.
33. Harata NC, Aravanis AM, Tsien RW (2006) *J Neurochem* 97:1546–1570.
34. An S, Zenisek D (2004) *Curr Opin Neurobiol* 14:522–530.
35. Alvarez de Toledo G, Fernandez-Chacon R, Fernandez JM (1993) *Nature* 363:554–558.
36. Fernandez JM, Neher E, Gomperts BD (1984) *Nature* 312:453–455.
37. Gandhi SP, Stevens CF (2003) *Nature* 423:607–613.
38. Aravanis AM, Pyle JL, Tsien RW (2003) *Nature* 423:643–647.
39. Maura G, Carbone R, Guido M, Pestarino M, Raiteri M (1991) *Eur J Pharmacol* 202:185–190.
40. Crispino M, Capano CP, Kaplan BB, Giuditta A (1993) *J Neurochem* 61:1144–1146.